World Academy of Science, Engineering and Technology
International Journal of Aerospace and Mechanical Engineering
Vol:6, No:12, 2012

Numerical Analysis and Sensitivity Study of Non-Premixed Combustion Using LES

J. Dumrongsak, and A. M. Savill

***Abstract*—**Non-premixed turbulent combustion Computational Fluid Dynamics (CFD) has been carried out in a simplified methane-fuelled coaxial jet combustor employing Large Eddy Simulation (LES). The objective of this study is to evaluate the performance of LES in modelling non-premixed combustion using a commercial software, FLUENT, and investigate the effects of the grid density and chemistry models employed on the accuracy of the simulation results. A comparison has also been made between LES and Reynolds Averaged Navier-Stokes (RANS) predictions. For LES grid sensitivity test, 2.3 and 6.2 million cell grids are employed with the equilibrium model. The chemistry model sensitivity analysis is achieved by comparing the simulation results from the equilibrium chemistry and steady flamelet models. The predictions of the mixture fraction, axial velocity, species mass fraction and temperature by LES are in good agreement with the experimental data. The LES results are similar for the two chemistry models but influenced considerably by the grid resolution in the inner flame and near-wall regions.

***Keywords*—**Coaxial jet, reacting LES, non-premixed combustion, turbulent flow.

I. Introduction

DUE to increasing environmental concerns and stringent emission regulations, modern combustion engineers designing a gas turbine combustor have to face the challenge of the optimisation of environmental emissions, combustion efficiency and stability. Accurate predictions of important physical and chemical properties of the combustion process are necessary in order to achieve improved combustor design with high efficiency and low emissions.

Combustion involves many complex phenomena, such as turbulence, recirculation, mixing, fuel chemistry, turbulence-chemistry interaction, heat and mass transfer. The chemical reaction takes place in a turbulent environment where the highly unsteady fluid motions of a wide range of length and time scales are present. Of particular interest is non-premixed combustion in a coaxial jet combustor configuration. It is simple yet manifests many complex flow features which are similar to those in a real gas turbine combustor.

Computational Fluid Dynamics (CFD) plays an important role in designing and optimising flow processes, especially in cases which experimental studies are not able to provide sufficient flow information due to the expensive setup cost or limitation in the measurement technology. In CFD, the combustion process is described by governing transport equations for fluid flow and heat transfer, along with models for combustion chemistry, radiation and other important sub-processes. Reynolds Averaged Navier-Stokes (RANS), a turbulence modelling approach in CFD, models all scales of motions and described flows in statistical sense. Large Eddy Simulation (LES), on the other hand, resolves the larger-scale eddies directly, while the smaller eddies and their interactions with the large-scale motions are modelled.

As the rate of the reaction in combustion depends on the mixing rate, numerical models employed must be able to capture the mixing and unsteady flow behaviours accurately to provide an insight into the combustion process, which is of practical and technical importance. In LES, the combustion process has to be modelled since the chemical reaction and heat release occur primarily at the smallest scales. However, by solving for the large, energy-containing scales of motions which dictate the behaviours of turbulent flows and the rate of mixing, the LES approach is expected to be superior to the RANS approach in capturing the turbulent combustion characteristics.

Some of the main approaches developed for modelling the turbulent combustion are the flamelet model [1], probability density function [2], linear eddy modelling [3], and conditional moment closure [4]. Although these concepts were first proposed in the context of RANS, many of these established combustion models have been extended to use in LES. Numerous studies have shown the capability of LES in reliably predicting scalar mixing, intermediate species and product formation in turbulent reacting flows with high fidelity.

The steady flamelet model was implemented with LES and tested in non-premixed combustion by Cook *et al.* [5]. The unsteady flamelet model employed in LES of a piloted jet diffusion flame by Pitsch and Steiner [6] was able to predict carbon monoxide (CO) with high accuracy. Pierce and Moin [7] proposed the steady flamelet/progress variable approach for LES and tested it in non-premixed turbulent combustion where good agreement with the experimental data was achieved. The unsteady flamelet/progress variable approach, which is an extension of Pierce and Moin's chemistry model [7], was proposed by Pitsch and Ihme [8] and implemented in LES of a confined swirl coaxial jet combustor. Mehesh *et al.* [9] applied the approach developed by Pierce and Moin [7] to gain an insight into the combustion process in a complex gas turbine combustor. Wang *et al.* [10] successfully incorporated

J. Dumrongsak is a PhD student in the Power and Propulsion Department, Cranfield University, Cranfield, Bedfordshire, MK430AW UK (phone: 44(0)1234-750111, fax: 44(0)1234-752462, email: j.dumrongsak@cranfield.ac.uk).

A. M. Savill is a Professor and the Head of Power and Propulsion Sciences within the Power and Propulsion Department, Cranfield University, Cranfield, Bedfordshire, MK430AW UK (e-mail: mark.savill@cranfield.ac.uk).

the fast chemistry model into LES of non-premixed combustion in simplified a coaxial jet combustor.

The purpose of this study is to evaluate the capability of LES in modelling non-premixed turbulent combustion employing a commercial software, FLUENT, and to test the sensitivity of the simulation results to the grid resolution and chemistry models. This paper is organised as follows. First, the mathematical formulation, including the flow governing equations and combustion models are presented. The numerical method and computational setup are described. The simulation results are presented, validated and discussed. Lastly, the findings are summarised in the conclusion.

II. Large Eddy Simulation

A. Governing Equations

In the LES approach, large-scale energy-containing motions are computed directly while the small-scale motions and their interactions with the large-scale eddies are represented by mathematical models. LES is three-dimensional and time-dependent. It involves the spatial filtering operation, which is defined as [11],

$$\bar{u}(x,t) = \int G(r,x)\, u(x-r,t)dr, \tag{1}$$

where the integration is performed over the entire flow domain, G is a low-pass filter function, usually a top-hat or Gaussian function, which satisfies the normalisation condition, $\int G(r,x)dr = 1$, and r is the radial coordinate. The filtering operation removes the instantaneous small-scale fluctuations and decomposes flow-field variables into the sum of filtered, resolved, components and residual, or subgridscale (SGS), components. The resolved components, which are three-dimensional and unsteady, represent the large-scale motions. Applying this procedure to the set of incompressible flow governing equations with chemical reaction yields the LES equations expressed as [12],

Continuity:

$$\frac{\partial \bar{u}_i}{\partial x_i} = 0 \tag{2}$$

Momentum:

$$\frac{\partial \bar{u}_j}{\partial t} + \frac{\partial \bar{u}_i \bar{u}_j}{\partial x_i} = -\frac{\partial \bar{p}}{\partial x_j} + \nu \frac{\partial^2 \bar{u}_j}{\partial x_i x_i} - \frac{\partial \tau_{ij}^{sgs}}{\partial x_i}, \tag{3}$$

Species Transport:

$$\frac{\partial \bar{Y}_\alpha}{\partial t} + \frac{\partial \bar{u}_i \bar{Y}_\alpha}{\partial x_i} = -\frac{\partial \bar{J}_i^\alpha}{\partial x_i} - \frac{\partial M_i^\alpha}{\partial x_i} + \bar{\omega}_\alpha, \tag{4}$$

where u_i and u_j denote the velocity vectors, p is the pressure, ν is the kinematic viscosity, Y_α represents the species' mass fractions, and ω_α denotes the chemical reaction term for species α (α = 1, 2,..., n). An over-bar denotes the filtering operation. The species mass flux, J_i^α, is represented by

$$J_i^\alpha = -\Gamma \frac{\partial Y_\alpha}{\partial x_i}, \tag{5}$$

where the diffusivity $\Gamma = \nu/Sc$, and Sc is the Schmidt number. The subgrid stress, τ_{ij}^{sgs}, subgrid species mass flux, M_i^α, and filtered chemical reaction term, $\bar{\omega}_\alpha$ are unclosed terms in the momentum and scalar transport equations which require closure modelling.

B. Subgrid Scale Modelling

The unresolved subgrid stress, $\tau_{ij}^{sgs} = \overline{u_i u_j} + \bar{u}_i \bar{u}_j$, which results from the filtering operation, represents the effects of the small scales on the resolved scales. The subgrid stress is modelled via the Boussinesq turbulent viscosity assumption [13]

$$\tau_{ij}^{sgs} = -2\nu_t \bar{S}_{ij} + \frac{1}{3}\delta_{ij}\tau_{kk}, \tag{6}$$

where $\bar{S}_{ij}$ is the filtered strain rate tensor defined by

$$\bar{S}_{ij} = \frac{1}{2}\left(\frac{\partial \bar{u}_i}{\partial x_j} + \frac{\partial \bar{u}_j}{\partial x_i}\right). \tag{7}$$

The turbulent viscosity, or eddy viscosity, ν_t, is given by the standard Smagorinsky model [14]

$$\nu_t = (C_s \Delta)^2 |\bar{S}|, \tag{8}$$

where the Smagorinsky coefficient, C_s, is an empirical constant, Δ is the filter width approximated by the cube root of the cell volume and the characteristic filtered strain rate $|\bar{S}| \equiv \left(2\bar{S}_{ij}\bar{S}_{ij}\right)^{1/2}$.

The subgrid species flux, $M_i^\alpha = \overline{u_i Y_\alpha} - \bar{u}_i \bar{Y}_\alpha$, is modelled as

$$M_i^\alpha = -\Gamma_t \frac{\partial \bar{Y}_\alpha}{\partial x_i}, \tag{9}$$

where the species turbulent diffusivity, $\Gamma_t = \nu_t/Sc_t$ and Sc_t is the turbulent Schmidt number.

III. Combustion Models

Chemical reactions in non-premixed combustion occur due to the molecular mixing of the initially separated fuel and oxidiser. The rate of reaction is typically controlled by the mixing rate. A very important scalar quantity used to describe the mixing rate of the fuel and oxidiser is the mixture fraction, Z, which is essentially the local mass fraction of the burnt and unburnt fuel [15]. Mixture-fraction-based approach, which assumes that the chemical reaction rate is faster than the mixing rate, forms the basis of most non-premixed combustion models.

For a system with one fuel stream, the mixture fraction is defined as [16]

$$Z = \frac{Y_\alpha - Y_{\alpha,O}}{Y_{\alpha,F} - Y_{\alpha,O}}, \quad (10)$$

where $Y_{\alpha,F}$ and $Y_{\alpha,O}$ represent the species mass fraction at the fuel and oxidiser stream inlets respectively. The value of Z is 1 in the fuel stream, 0 in the oxidiser stream, ranges between 0 and 1 depending on the amount of mixing which has occurred. Because Z is a conserved scalar which is independent of the chemistry, there is no source term in its governing transport equation and the combustion is simplified to a mixing problem. The mixture fraction transport equation for incompressible flows can be written as [17],

$$\frac{\partial \bar{Z}}{\partial t} + \frac{\partial \bar{u}_i \bar{Z}}{\partial x_i} = -\frac{\partial \bar{J}_{z,i}}{\partial x_i} - \frac{\partial M_{z,i}}{\partial x_i}, \quad (11)$$

where $J_{z,i}$ denotes the mixture fraction mass flux and $M_{z,i}$ is the subgrid mixture fraction mass flux which requires closure modelling as similar to M_i^α.

A. Equilibrium Chemistry

The equilibrium chemistry assumes that the reactions are infinitely fast but reversible. At each value of the mixture fraction, all species are in chemical equilibrium. The instantaneous mass fractions of these species can be calculated as functions of the mixture fraction as [18]-[19],

$$Y_\alpha = Y_\alpha^e(Z), \quad (12)$$

where e denotes equilibrium. Similar equations can be written for the equilibrium temperature and density, ρ.

B. Probability Density Function

Non-premixed combustion modelling involves solving the mixture fraction transport equation instead of the individual species transport equations. The species concentrations can then be derived from the predicted mixture fraction. The instantaneous relationships between the mixture fraction and the species mass fractions are given under equilibrium chemistry assumption in (12). The instantaneous values in the chemical state relationship and the filtered values are linked by the interaction of turbulence and chemistry which is usually accounted for by the probability density function (PDF) approach. This relationship can be expressed as [20]-[22],

$$\bar{Y}_\alpha = \int_0^1 Y_\alpha^e(Z)\bar{f}(Z)dZ. \quad (13)$$

The filtered density function, $\bar{f}(Z)$, describes the statistical properties of the fuel and air mixing by quantifying the probability of finding $\bar{Y}_\alpha$for a given spatial point, x, and time, t. The $\bar{f}(Z)$ is unknown and requires modelling. The actual shape of $\bar{f}(Z)$ can be approximated by a mathematical model which assumes beta-functiondistribution expressed as a function of $\bar{Z}$ and its variance, $\overline{Z'^2}$ [23]-[25],

$$\bar{f}(Z) = \frac{Z^{a-1}(1-Z)^{b-1}}{\int_0^1 Z^{a-1}(1-Z)^{b-1}dZ} \quad (14)$$

where

$$a = \bar{Z}\left[\frac{\bar{Z}(1-\bar{Z})}{\overline{Z'^2}} - 1\right] \quad (15)$$

and

$$b = (1-\bar{Z})\left[\frac{\bar{Z}(1-\bar{Z})}{\overline{Z'^2}} - 1\right] \quad (16)$$

For LES, the mixture fraction variance is modelled as,

$$\overline{Z'^2} = C_v L_s^2 |\nabla \bar{Z}|^2, \quad (17)$$

where L_s is the subgrid length scale and C_v is a constant which is set to be 0.5 in this study. Given the predictions of $\bar{Z}$ and $\overline{Z'^2}$, the filtered species mass fraction, density and temperature can be determined. In FLUENT, these integrals are preprocessed once and stored in look-up tables in the library, making this method highly computational efficient. This concept is demonstrated in Fig. 1 which shows the filtered temperature solutions stored in the equilibrium chemistry library for the methane-air combustion at 750 K air, 300 K fuel and 3.8 atm.

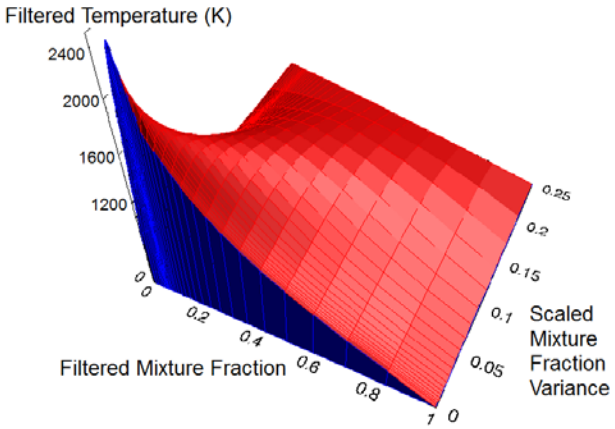

Fig. 1 Temperature solutions from the equilibrium chemistry library for the methane-air combustion at 750 K air, 300 K fuel and 3.8 atm

C. Flamelet Models

The flamelet models assume that the chemical reactions are fast enough that they occur in a thin layer near the stoichiometric mixture on a scale smaller than the Kolmogorov scale. As a result, the structure of the reaction zone remains laminar and the diffusive transport occurs in the normal direction to the surface of the stoichiometric mixture. Therefore, the scalar transport equations can be written such that the mixture fraction is an independent coordinate [1], [26],

$$\frac{\partial Y_\alpha}{\partial t} = \frac{1}{2}\rho\chi\frac{\partial^2 Y_\alpha}{\partial Z^2} + \omega_\alpha. \quad (18)$$

For the steady laminar flamelet model, the flame structure is assumed to be in the steady state and the first term on the left hand side in (18), which is the time derivative, can be neglected. The scalar dissipation rate, χ, is defined as $\chi = 2D|\nabla Z|^2$, where D is the scalar diffusivity which represents the local mixing rate. Where fl denotes flamelet, st represents stoichiometry, the relationship between Z and χ is assumed to be [1]

$$Y_\alpha = Y_\alpha^{fl}(Z, \chi_{st}). \quad (19)$$

The filtered species mass fraction, as well as the temperature, can be obtained from the integral,

$$\bar{Y}_\alpha = \int_0^1 Y_\alpha^{fl}(Z, \chi_{st})\tilde{f}(Z, \chi_{st})dZd\chi_{st}. \quad (20)$$

It is assumed that Z and $\chi_{st}$are statistically independent [1]. Therefore, the joint PDF, $f(Z, \chi_{st})$, can be simplified to $f(Z)f(\chi_{st})$. As similar to the equilibrium chemistry, the integrations in (20) are pre-calculated and stored in the look-up tables. The shape of $f(Z)$ is assumed to be that of the beta-function distribution and is a function of $\bar{Z}$ and $\overline{Z'^2}$. The PDF of χ is described by a delta-function, ignoring the fluctuations. For LES, the filtered scalar dissipation is modelled as,

$$\overline{\chi_{st}} = C_\chi \frac{(\mu_t+\mu)}{\rho\sigma_t}|\nabla\bar{Z}|^2, \quad (21)$$

whereμ is dynamic viscosity, μ_t is turbulent dynamic viscosity, C_χ and σ_t are constants with the values of 2 and 0.85 respectively.

IV. Numerical Methods and Computational Setup

The numerical studyhas been carried out in FLUENT for a coaxial jet combustor with the configuration and operating conditions similar to that in the experiment of Owen *et al.* [27]. The central inflow is a pure methane stream with a velocity of 0.9287 m/s. The annular inflow is a non-swirling air stream with a bulk velocity,U, of 20.63 m/s. The operating pressure of the combustor is 3.8 atm. The temperature of the fuel and air are 300 K and 750 K respectively. The two inflow streams are separated by a thin splitter plate with the thickness of 0.018 cm. The centre radius, annular outer radius, R, and combustor radius are 3.157 cm, 4.685 cm and 6.115 cm accordingly. The domain extends at a distance of 0.2R upstream and the length of the combustor is 8.1R.

Two O-type meshes of 2.3 and 6.2 million grid cells are created for the grid sensitivity analysis. These will hereinafter be referred to as the coarse and fine grids respectively. The grid is clustered in the axial direction near the jet exit and in the radial direction near the splitter plate wall to capture the rapid changes of flow properties in these regions. The schematic of the computational grid employed in this study is shown in Fig. 2. The flow goes from left to right. The upstream boundary is specified as multiple velocity inlets. The fuel inlet is a fully developed pipe flow with velocity described by the 1/7th power law. The downstream boundary is specified as pressure outlet. All solid boundaries, including the splitter plate, are specified as walls and assumed to be adiabatic and impermeable.

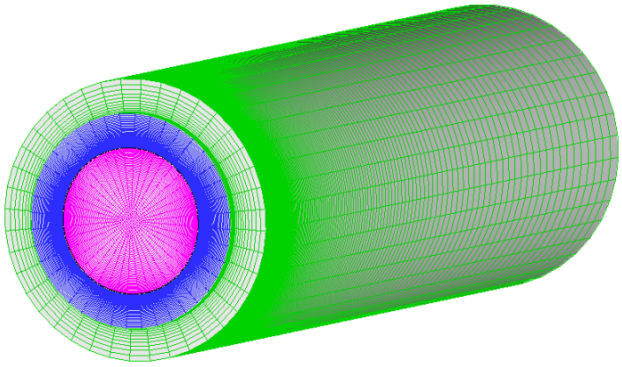

Fig. 2 Schematic of the computational grid

Turbulence modelling approaches employed in the study are LES and RANS k-epsilon. For LES, the unresolved subgrid scales are treated with the standard Smagorinsky-Lilly model. The chemistry models compared in the LES sensitivity study are the equilibrium and steady flamelet models. Only the equilibrium chemistry is employed in the LES grid sensitivity study. The filtered transport equations are spatially discretised using the finite volume method. The momentum equations are solved applying the bounded central differencing scheme. The second order upwind scheme is used to solve the filtered mixture fraction transport equation. The time step employed in LES is 10^{-5}. To allow for the initial flow development, the simulations has been performed for 220R/U seconds before sampling data are collected for another 1760R/U seconds to ensure adequately converged statistics are obtained.

For validation, the simulation results from this study are compared with the experimental measurements of Owen *et al.* [27] and previous LES calculation by Pierce and Moin[7], who developed and employed the steady flamelet/progress variable chemistry model with a computational grid of approximately 2.5 million cells. The results validated are the profiles of chemical species in mass fraction, temperature and axial velocity at various stations inside the combustor. The length and velocity presented are normalised by R and U respectively.

V. Results and Discussion

A. LES and RANS

Simulations have been performed employing current LES and RANS with the coarse grid and the equilibrium chemistry model to compare the capability of the transient and steady turbulence modelling approaches in capturing the flame structure. Fig. 3 compares the mixture fraction contours on the mid plane predicted by LES and RANS. The LES approach,

which provides instantaneous flow fields, predicts asymmetric mixing behaviour at this instance with more mixing on the upper side than the lower side of the fuel port. Since RANS is able to provide only the mean flow fields, the mixture fraction contours obtained are smooth and symmetric which is unrealistic. The initial thin mixing layers near the splitter plate predicted by both LES and RANS indicate weak mixing. This is due to the high chemical heat release rates produced by the equilibrium model which push the fuel and oxidiser apart, thus reducing the mixing rate in this region.

The corresponding contours of product mass fraction are shown in Fig. 4. Product mass fraction is calculated from the sum of carbon dioxide (CO_2) and water vapour (H_2O) mass fractions. The regions with high product concentration mark the flame location. The LES approach is able to provide more detailed flow information and predicts highly unsteady flame behaviours as indicated by irregular, wavy contours which agree with the flame behaviours observed in the experiment [27]. At the instance shown, more products are formed in the upper region near the fuel port than the lower region which is consistent with the mixture fraction predictions. It is also shown that some unburnt reactants are able to penetrate into the flame. The RANS approach, on the other hand, predicts symmetric flame. Both LES and RANS predict flame attached to the splitter plate. For this case, the highest production mass fraction attainable in theory is approximately 0.275 which occurs at the stoichiometric mixture fraction [7]. It is illustrated in Fig. 4 that the RANS approach under-predicts the product mass fraction significantly.

To further demonstrate the qualitative comparison shown in Fig. 3, the mixture fraction profiles predicted by LES and RANS are compared in Fig. 5. The predictions form LES are time-averaged. At the station x/R = 0.21 near the splitter plate, the LES approach offers improvement over the RANS approach which under-predicts the mixing rate significantly. At the downstream station x/R = 3.84, RANS still under-predicts the mixing rates. LES, on the other hand, over-predicts the mixing rate and produces the mixture fraction profile which is almost level, suggesting that the mixing is almost complete at this station. The mixture fraction profile from the modified LES [7] agrees very well with the experimental data at this station. The RANS approach predicts the mixture fractions near the wall with slightly higher fidelity than the LES approach which is known to experience difficulties predicting the near-wall flows accurately [13], [28]-[30]. This is because LES requires grid to be sufficiently fine to resolve the flow in viscous near-wall regions.

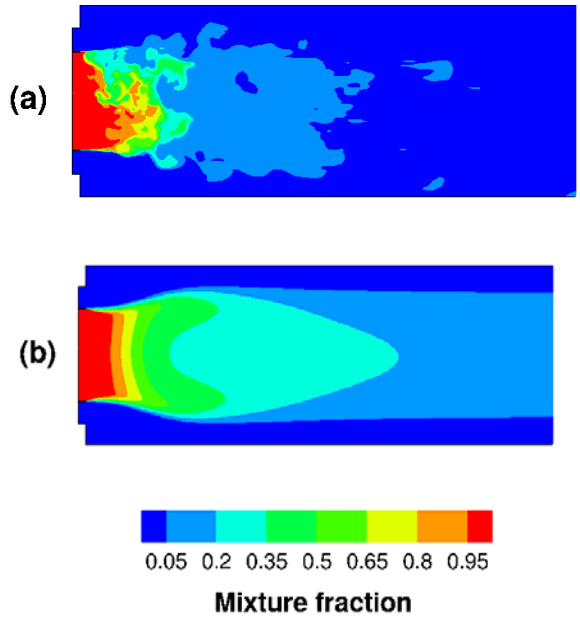

Fig. 3 Mixture fraction contours from (a) LES and (b) RANS

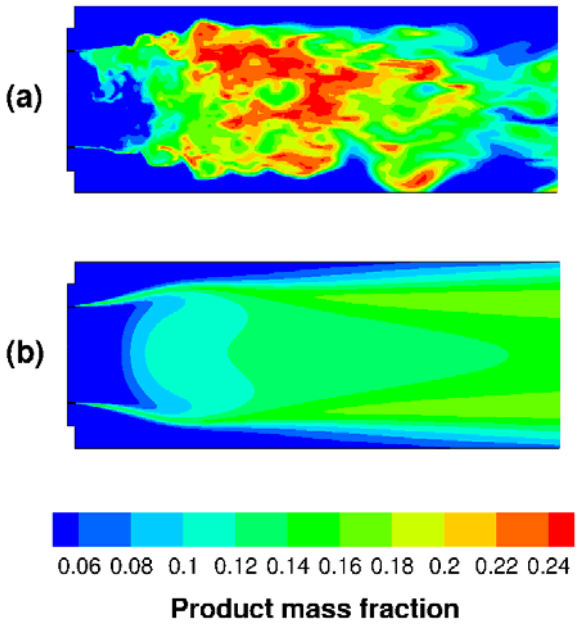

Fig. 4 Product mass fraction contours from (a) LES and (b) RANS

Fig. 6 compares the temperature profiles predicted by LES and RANS. At the upstream station x/R = 0.89, the temperature profile predicted by LES agrees better with the experimental data than RANS in the inner and mixing regions. However, the LES predictions deviate from the experimental data more than the RANS predictions in the near-wall region. The sharp peak in the mixing layer predicted by RANS corresponds to the attached flame at the splitter plate shown in Fig. 4(b) and lower mixing rates illustrated in Fig. 5. The flame predicted by RANS remains attached to the splitter plate at downstream station x/R = 1.57 as indicated by a spike in the temperature profile. The temperature profile predicted by current LES agrees generally well with the experimental data in the inner flame region. However, as similar to the upstream station, the current LES results in the near-wall region deviate from the experimental measurements considerably.

The axial profiles of temperature along the centerline of the combustor predicted by LES and RANS are shown in Fig. 7.

Both temperature profiles start inside the fuel port at fuel temperature of 300 K. The temperature predicted by LES increases inside the fuel port and continues to increase inside the combustor. This indicates that for current LES, the mixing and, thus, reaction takes place right after the fuel port and there is a recirculation of hot products inside the fuel port. The temperature gradient predicted by LES is steeper than that by RANS. The mixing and reaction predicted by RANS start approximately at the distance 0.4 radii downstream. RANS also constantly predicts lower temperature than LES.

Fig. 8 shows the axial profiles of temperature along the splitter plate line predicted by LES and RANS. High temperature spikes right after the splitter plate predicted by both turbulence models correspond to the attached flames illustrated in Fig. 4. This is due to the deficiencies of the equilibrium chemistry model which is not able to account for the non-equilibrium effects such as the flame lift-off in this region. However, the attached flame predicted by RANS is more intense than that predicted by LES as indicated by the higher temperature and longer attached flame distance. The temperature drops and rises again due to the mixing and reaction. RANS again consistently predicts lower temperature than LES because it predicts weaker mixing.

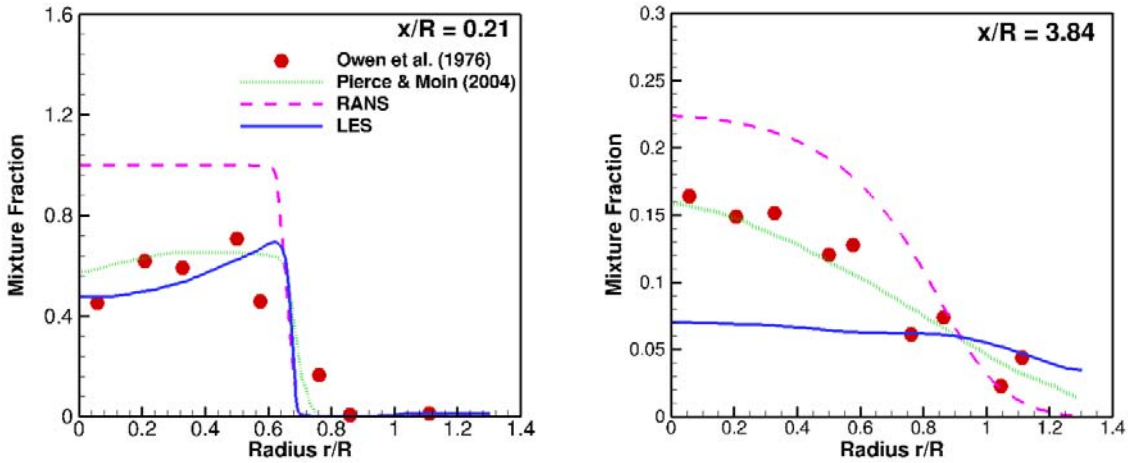

Fig. 5 Profiles of mixture fraction from LES and RANS

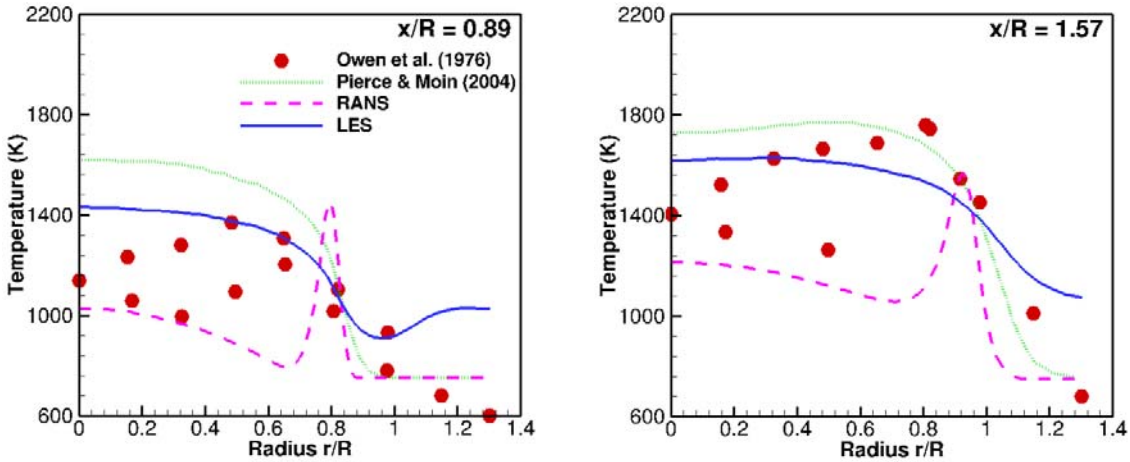

Fig. 6 Profiles of temperature from LES and RANS

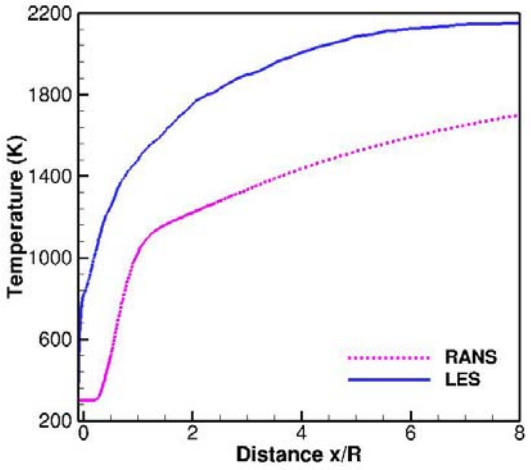

Fig. 7 Axial profiles of temperature along the centerline of the combustor from LES and RANS

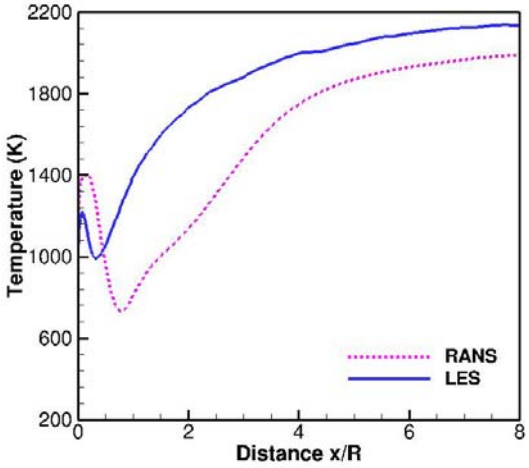

Fig. 8 Axial profiles of temperature along the splitter plate line from LES and RANS

B. LES Flame Structure

The flame structure is illustrated in Fig. 9 which shows the instantaneous temperature iso-surfaces and radial cross sectional contours predicted by current LES with the fine grid and the equilibrium chemistry model. The regions with high temperature represent the flame location. As shown in Fig. 9(a), the flame is contained in the central region behind the fuel port and extends in the axial direction along the combustor length. This is consistent with the flame configuration observed in the experiment [27]. The re-circulating combustion products caused by the high air-to-fuel velocity ratio provided a continuous ignition source and stabilised the flame. The flame in the experiment lifted off from the rim of the nozzle and reattached intermittently in an extremely unsteady manner. However, in this study, the flame is predicted to be attached to the splitter plate. This is due to the incapability of the equilibrium chemistry and steady flamelet models in capturing non-equilibrium effects such as extinction, ignition and flame lift-off.

For the radial cross sectional contours of the temperature illustrated in Fig. 9(b), the upstream locations show distinct temperature zones. The cold annular air stream is forced outward towards the wall by the reaction and forms a lower temperature layer which enfolds the inner higher temperature region. The thickness of this layer of cold air reduces as the axial distance increases. The flame is made up of separate high temperature zones within the fuel-air shear layer region. The size of high temperature zones is small upstream, near the fuel port but increases and the segregated zones become more amalgamated as the axial distance increases.

C. Mixture Fraction

To assess the sensitivity of the LES solutions to the grid resolution, LES is performed on the coarse and fine grids employing only the equilibrium chemistry model. The effects of the chemistry model employed on the LES results are evaluated by employing the equilibrium and steady flamelet models on the coarse grid. Fig. 10 shows the time-averaged mean mixture fraction profiles obtained from the simulations. Since the temperature, density and other species mass fractions are derived from the mixture fraction, it is important to accurately predict the profiles of mixture fraction.

At the station x/R = 0.21, the simulation results agree generally well with the experimental data. The equilibrium and steady flamelet models produce similar mixture fraction profiles. Both chemistry models predict slightly lower mixing rates in the mixing layers than those in the experiment. The current LES results are insensitive to the grid density at this station. At the stations x/R = 3.16 and 3.84, there is a significant under-prediction of the mixture fraction by both chemistry models with the coarse grid. This can be the result of low grid resolution employed in this region. As illustrated in Fig. 10, the current LES predictions improve when the grid is refined, especially in the central and near-wall regions. The predictions from modified LES with more advanced chemistry modeling approach [7], on the other hand, are in excellent agreement with the experimental data at these stations.

The instantaneous iso-surfaces of the mixture fraction predicted by current LES on the coarse and fine grids are shown in Fig. 11. Qualitative comparison reveals the fine grid is able to capture more smaller-scale mixing especially in the upstream region near the fuel port.

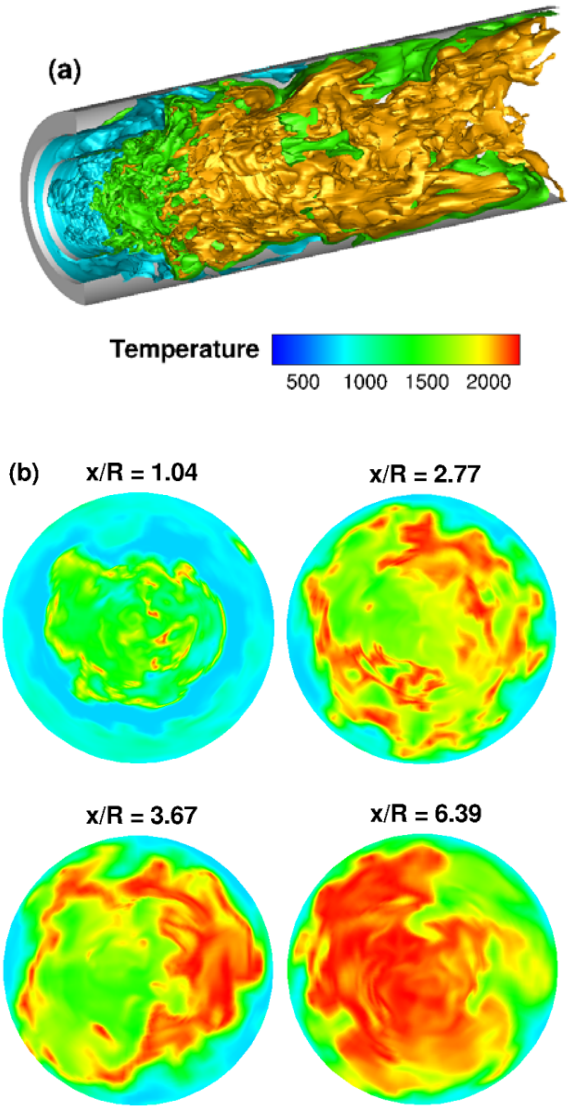

Fig. 9 Instantaneous temperature (a) iso-surfaces and (b) radial cross sectional contours from LES with the fine grid

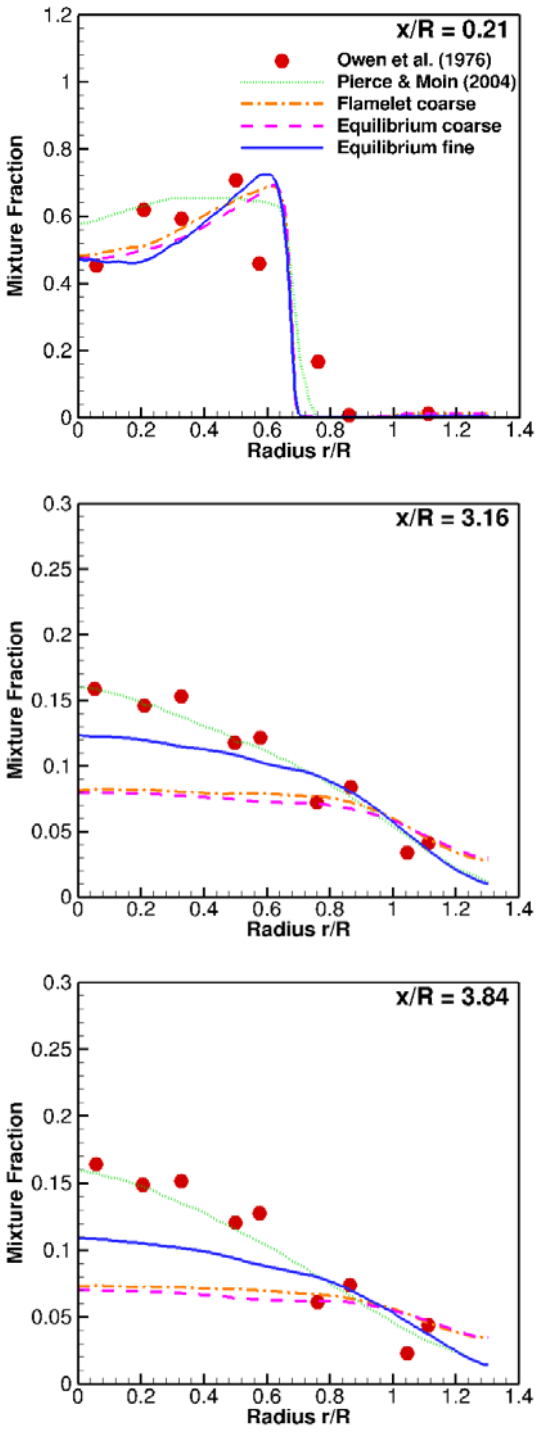

Fig. 10 Profiles of time-averaged mixture fraction

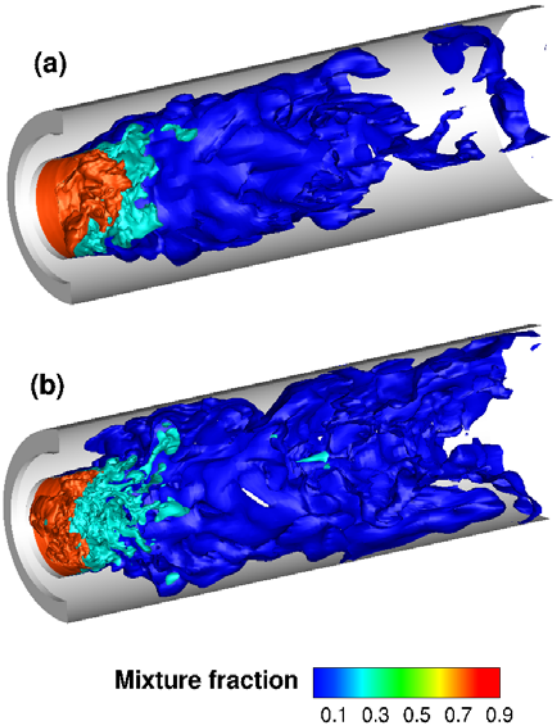

Fig. 11 Instantaneous mixture fraction iso-surfaces (a) from the coarse and (b) fine grids

D.Product Mass Fraction

The profiles of time-averaged product mass fraction are shown in Fig. 12. The equilibrium and steady flamelet models predict a spike in the thin mixing layers near the splitter plate at the station x/R = 0.21. High product formation predicted in this region by both chemistry models corresponds to the attached flame shown in Fig. 4 and Fig. 9(a) and low mixing rates illustrated in Fig. 10.The products found in the inner region are the results of the recirculation from the reaction downstream. In this region, the steady flamelet models predict higher product mass fractions than the equilibrium chemistry. Furthermore, both chemistry models predict higher product mass fractions near the wall. These discrepancies are reduced considerably when the grid resolution increases. At the stations x/R = 3.16 and 3.84, the simulation results from both chemistry models are in good agreement with the experimental data. Improvement in the near-wall predictions again, can be observed when the finer grid is employed.

E. Temperature

Fig. 13 shows the profiles of time-averaged temperature. There is a good agreement between the predicted temperature profiles from both chemistry models and the experimental measurements. Discrepancies between the predicted near-wall temperature and the experimental data at all stations shown are due to the adiabatic wall assumption applied in the study. In the experiment, the combustor wall was isothermal, cooled to the temperature of approximately 500 K. Therefore, the near-wall temperature can be affected by the thermal boundary layers which have been developed. However, as shown in Fig. 13, the temperature predictions near the wall can still be improved when the grid is refined.

F. Carbon Monoxide Mass Fraction

The time-averaged profiles of CO mass fraction are shown in Fig. 14.At the station x/R = 0.21, the equilibrium model predicts a spike in CO mass fraction in the mixing layers as similar to the product mass fraction predictions. However, there is no such peak in the CO mass fraction predicted by the steady flamelet model. At the station x/R = 3.84, there are large discrepancies between the results from both chemistry models and the experimental data. This deviation reduces especially in the inner region when the fine grid is employed.

G.Axial Velocity

Fig. 15and Fig. 16 show the profiles of time-averaged axial velocity and root-mean-square (RMS) velocity respectively. Although the mixture fraction is sensitive to the rates of chemical heat release, the predictions of axial velocity and its RMS are found to be rather insensitive to the chemistry models. This is also because the effects of the heat release on the velocity field are likely to be accumulative. At the station x/R = 0.14, the axial velocity profiles from the equilibrium and steady flamelet models are almost identical with slight improvement in the near-wall predictions when the fine grid is employed. At the station x/R = 1.27, there are large discrepancies between the predicted axial velocities in the inner region from both chemistry models and the experimental data. The recirculation in this region is not well captured by current LES. However, the modified LES with more advanced chemistry model [7] is able to predict axial velocity profile with good accuracy at this station.

VI. Conclusion

The findings from this study have demonstrated the superiority of LES in capturing the flame behaviours and flow characteristics of non-premixed turbulent combustion. Despite a simple chemistry model employed, LES is still able to outperform RANS in capturing unsteady flame structures and profiles of species mass fraction, temperature and velocity. This is because LES directly resolves the large-scale motions, which control the rate of mixing and reaction. The LES solutions obtained from the two chemistry models are similar except the upstream species mass fractions where the predictions differ slightly in the inner flame and near-wall regions. Discrepancies between the LES predictions and the experimental data are the results of the simple chemistry models employed not being able to cope with the rapid changes in the chemistry and take into account the non-equilibrium effects of the flame. However, the deviations of the LES predictions from the experimental data reduce as the computational grid is refined. As demonstrated by the results, the current LES calculations are found to be highly sensitive to the grid resolution, especially in the inner and near-wall regions. Nevertheless, as important aspects of the combustion process, such as the main reactions and pollution formation usually take place far away from the wall, sufficiently accurate LES predictions for future engineering applications can be achieved with an acceptable level of grid refinement.

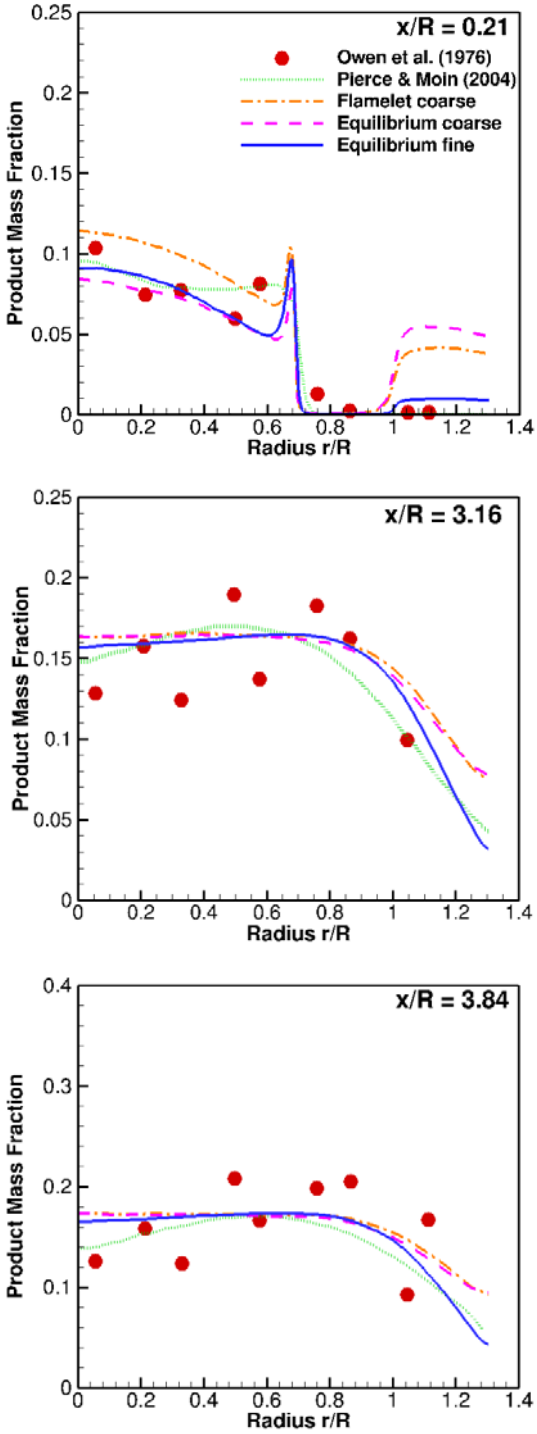

Fig. 12 Profiles of time-averaged product mass fraction

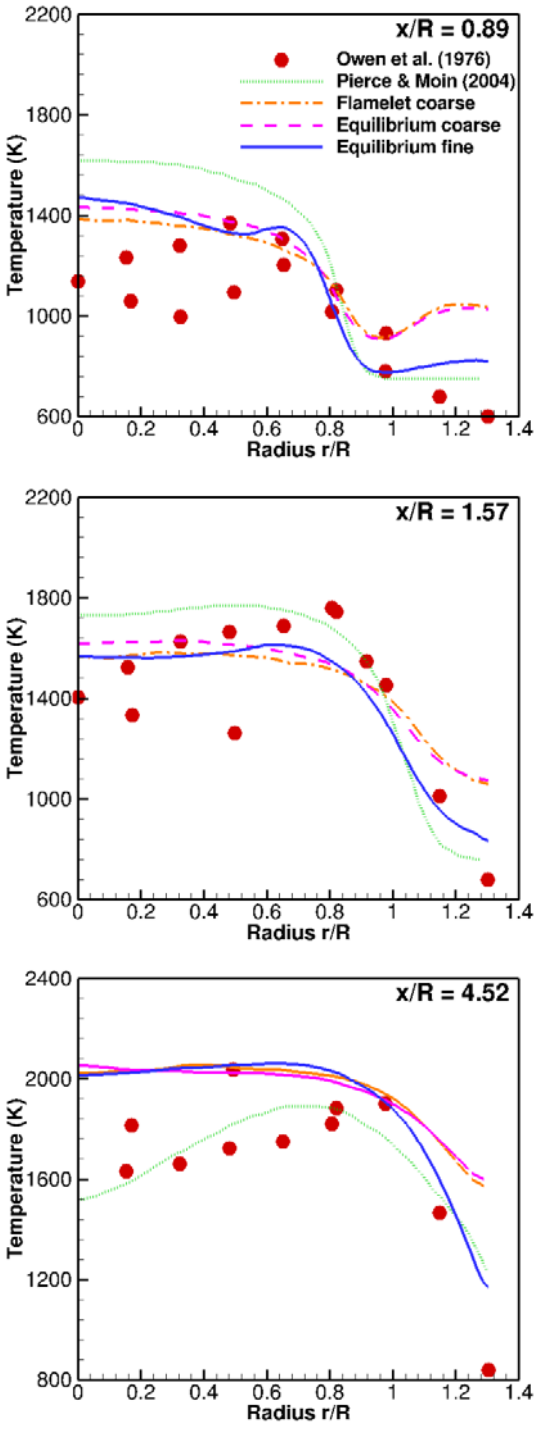

Fig. 13 Profiles of time-averaged temperature

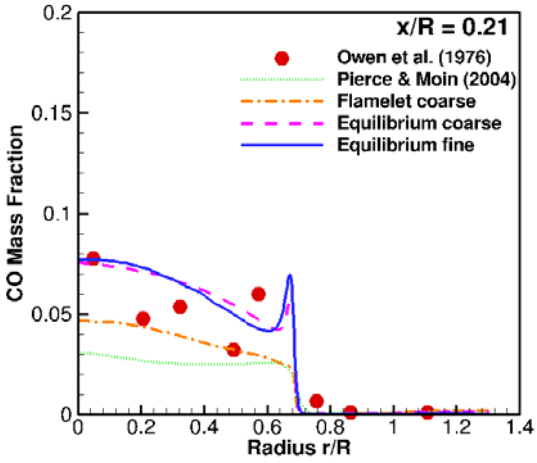

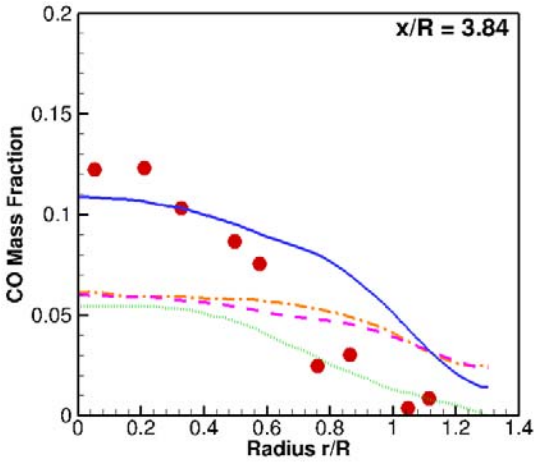

Fig. 14 Profiles of time-averaged CO mass fraction

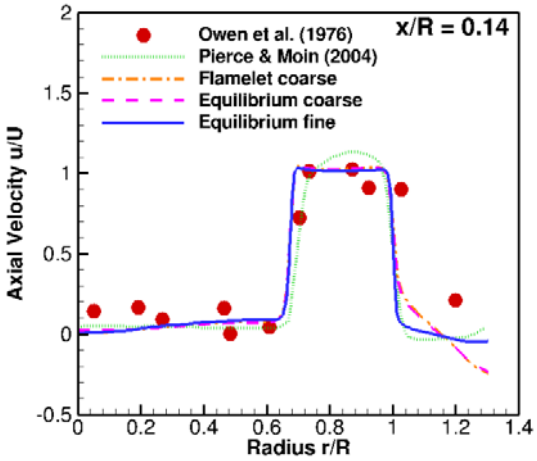

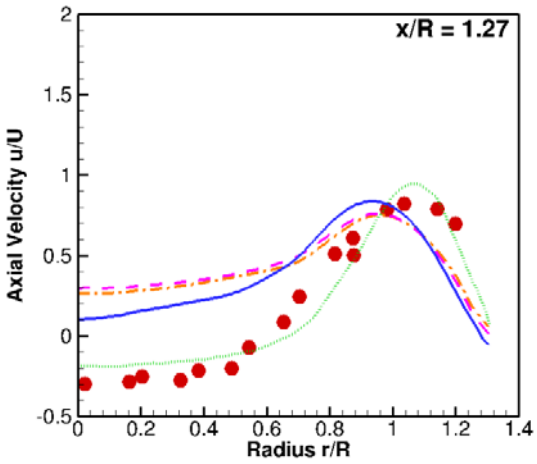

Fig. 15 Profiles of time-averaged normalised axial velocity

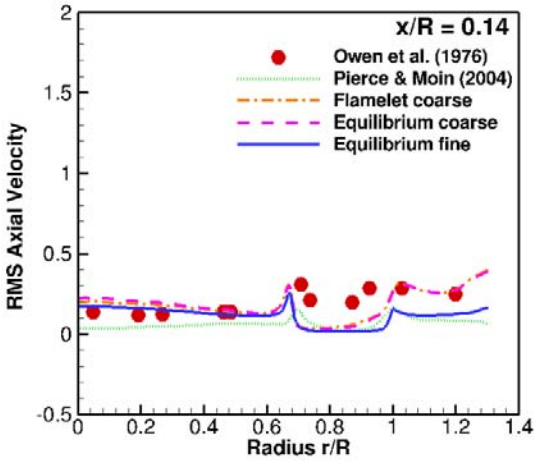

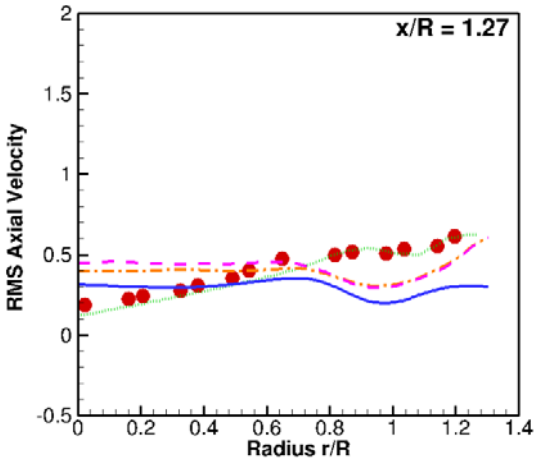

Fig. 16 Profiles of time-averaged RMS axial velocity

ACKNOWLEDGMENT

The author would like to thank the EU Clean Sky programme for the research funding. The author is also very grateful to her beloved mother and family for their unconditional support.

REFERENCES

[1] N. Peters, "Laminar diffusion flamelet models in non-premixed turbulent combustion,"*Prog. Energy Comb.Sci*., vol. 10, no. 3, pp. 319-339, 1984.

[2] S. B. Pope, "PDF methods for turbulent reactive flows," *Prog. Energy and Comb. Sci*., vol. 11, no. 2, pp. 119-192, 1985.

[3] A. R. Kerstein, "Linear-eddy modelling of turbulent transport. Part7. Finite-rate chemistry and multi-stream mixing," *J. Fluid Mech.*, vol. 240, pp. 289-313, 1992.

[4] A. Y. Klimenko and R. W. Bilger, "Conditional moment closure for turbulent combustion," *Prog. Energy Comb. Sci.*, vol. 25, no. 6, pp. 595-687, 1999.

[5] A. W. Cook, J. J. Riley, and G. Kosaly, "A laminar flamelet approach to subgrid-scale chemistry in turbulent flows," *Combustion and Flame*, vol. 109, pp. 332-341, 1997.

[6] H. Pitsch and H. Steiner, "Large-eddy simulation of a turbulent piloted methane/air diffusion flame (Sandia flame D)," *Phys. Fluids*, vol. 12, no. 10, pp. 2541-2554, 2000.

[7] C. D. Pierce and P. Moin, "Progress-variable approach for large-eddy simulation of non-premixed turbulent combustion," *J. Fluid Mech.*, vol. 504, pp. 73-97, 2004.

[8] H. Pitsch and M. Ihme, "An Unsteady/Flamelet Progress Variable Method for LES of Nonpremixed Turbulent Combustion," in *the43rd AIAA Aerospace Sciences Meeting and Exhibit*, Nevada, 2005.

[9] K. Mahesh, G. Constantinescu, S. Apte, G. Iaccarino, F. Ham, and P. Moin, "Large-eddy simulation of reacting turbulent flows in complex geometries," *Journal of Applied Mechanics*, vol. 73, pp. 374-381, 2006.

[10] K. Wang, Z. Yang, and J. J. McGuirk, "Large eddy simulation of turbulent diffusion flame combustion using a conserved scalar methodology," *Journal of Aerospace Power*, vol. 22, no. 7, pp. 1106-1117, 2007.

[11] A. Leonard, "Energy Cascade in Large-eddy Simulations of Turbulent Fluid Flows," *Adv. Geophys*., vol. 18A, pp. 237-248, 1974.

[12] P. J. Colucci, F. A. Jaberi, P. Givi, and S. B. Pope, "Filtered density function for large eddy simulation of turbulent reacting flows," *Phys. Fluids*, vol. 10, pp. 499-515, 1998.

[13] S. B. Pope, *Turbulent Flows*, New York: Cambridge University Press, 2000, ch. 13.

[14] J. Smagorinsky, "General circulation experiments with the primitive equations: I. The basic experiment," *Monthly Weather Review*, vol. 91, no. 3, pp. 99-164, 1963.

[15] H. Pitsch, "Large-eddy simulation of turbulent combustion," *Annu. Rev. Fluid Mech.*, vol. 38, pp. 453-482,2006.

[16] Y. R. Sivathanu and G. M. Faeth, "Generalized state relationships for scalar properties in non-premixed hydrocarbon/air flames," *Combustion and Flame*, vol. 82, pp. 211-230, 1990.

[17] N. Peters, *Turbulent Combustion*, Cambridge, UK: Cambridge University Press, 2000, ch. 3.

[18] R. W. Bilger, "Turbulent jet diffusion flames," *Prog. Energy and Comb. Sci*., vol. 1, pp. 87-109, 1976.

[19] R.W. Bilger, "Turbulent flows with nonpremixed reactants," in: *Topics in Applied Physics*, vol. 44, P. A. Libby and F. A. Williams, Eds. New York: Springer-Verlag, 1980, pp. 65-113.

[20] P. A. Libby and F. A. Williams, "Fundamental aspects," in: *Topics in Applied Physics*, vol. 44, P. A. Libby and F. A. Williams, Eds. New York: Springer-Verlag, 1980, pp. 1-43.

[21] E. E. O'Brien, "The probability density function (pdf) approach to reacting turbulent flows," in: *Topics in Applied Physics*, vol. 44, P. A. Libby and F. A. Williams, Eds. New York: Springer-Verlag, 1980, pp. 185-218.

[22] S. B. Pope, "Pdf method for turbulent reacting flows," *Prog. Energy Combust. Sci.*, vol. 11, pp. 119-195, 1985.

[23] R. P. Rhodes, P. T. Harsha, and C. E. Peters, "Turbulent kinetic energy analyses of hydrogen-air diffusion flames," *ActaAstronautica*, vol. 1, pp. 443-470, 1974.

[24] W. Kolbe and W. Kollmann, "Prediction of turbulent diffusion flames with a four-equation turbulence model," *ActaAstronautica*, vol. 7, pp. 91-104, 1980.

[25] A. W. Cook and J. J. Riley, "A subgrid model for equilibrium chemistry in turbulent flow," *Phys. Fluids*, vol. 6, pp. 2868-2870, 1994.

[26] N. Peters, "Local quenching due to flame stretch and non-premixed turbulent combustion," *Combust. Sci. Technol.*, vol. 30, pp. 1-17, 1983.

[27] F. K. Owen, L. J. Spadaccini, and C. T. Bowman, "Pollutant formation and energy release in confined turbulent diffusion flames,"*Proc. Combust. Inst*., vol. 16, pp. 105-117, 1976.

[28] J. A. Langford and R. D. Moser, "Optimal LES formulations for isotropic turbulence," *J. Fluid Mech.*, vol. 398, pp. 321-346, 1999.

[29] P. Sagaut, *Large Eddy Simulation for Incompressible Flows*, Berlin: Springer, 2001, ch. 10.

[30] B. Wegner, A. Maltsev, C. Schneider, A. Sadiki, A. Dreizler, and J. Janika, "Assessment of unsteady RANS in predicting swirl flow instability based on LES and experiments," *Int. J. Heat Fluid Flow*, vol. 25, no. 3, pp. 528-536, 2004.